Simulation of temperature influence on shear stress during mineral oil flow

Tomáš Polášek[1,*], *Marian* Ledvoň[1], *Adam* Bureček[1] and *Lumír* Hružík[1]

[1]VŠB -Technical University of Ostrava, Faculty of Mechanical Engineering, Department of Hydromechanics and Hydraulic Equipment, 708 00 Ostrava, Czech Republic

Abstract. The article is focused on the mathematical simulation of temperature influence on the shear stress during the mineral oil flow. The rotary rheometer is used to measure the shear stress. It works on the principle of torque measurement when the spindle rotates in the container with the measured liquid. The rotating spindle together with the container forms the hollow cylinder which is filled by measured oil. The shear stress is evaluated for the various oil temperatures. The software ANSYS Fluent is used to evaluate the partial numerical simulations. The experimental evaluation of the oil physical properties depending on the temperature is described in the article.

1 Introduction

If the fluid flows and its two adjacent layers have different velocities, the friction and the shear stress τ occur at their interface. The cause of this phenomenon is fluid viscosity η. The single flow streamlines are parallel during the laminar flow and the fluid does not mix. The following equation applies to this flow:

$$\tau = \eta \cdot \frac{d\gamma}{dt}, \tag{1}$$

where τ is the shear stress, η is dynamic viscosity and $\mathrm{d}\gamma/\mathrm{d}t$ is shear rate.

The shear stress τ is linearly proportional to the shear rate $\mathrm{d}\gamma/\mathrm{d}t$ according to this law. The dynamic viscosity η is given by the ratio of the shear stress τ and the shear rate $\mathrm{d}\gamma/\mathrm{d}t$.

The ratio of shear stress τ and shear rate $\dot{\gamma} = \mathrm{d}\gamma/\mathrm{d}t$ is constant for the Newtonian liquid.

For the non-Newtonian liquid, the ratio is not constant and this ratio is called the apparent viscosity.

The dependence of shear stress τ on the shear rate $\dot{\gamma}$ is called the flow curve. The flow curves are determined experimentally on the rheometers. The type of liquid can be determined according to the flow curve.

2 Experimental measurement

The physical properties are determined for the mineral oil sample type HV VG46. The dependence of the dynamic viscosity η_O, the shear stress τ_O and the density ρ_O of the mineral oil on the temperature t_O is evaluated. The measurement is performed for the oil temperature range $t_O = (10 \div 80)$ °C. The mineral oil is the most widespread liquid using in the hydrostatic systems nowadays [1].

2.1 Description of experimental measurement

The rotary rheometer Brookfield LVDV-II+Pro is used to determine the dependence of the oil dynamic viscosity η_O on the temperature t_O. The spindle rotates in the container where is situated the measured oil. The oil flows in the gap between the spindle and the inner container wall due to the spindle rotation. The rotating spindle together with container forms volume which has the hollow cylinder shape.

The dependence of the oil shear stress τ_O and the spindle torque T on the oil temperature t_O is also determined using this rheometer. The generated torque T on the rotating spindle is absorbed by the calibrated spring. The spindle torque T range must be within the range $T_{\%} = (10 \div 100)$ % to ensure the measurement accuracy. The percentage value $T_{\%} = 100\%$ corresponds to the torque value $T = 0.0673$ mN·m [2]. The torque value T can be corrected using the speed s change respectively the shear rate $\dot{\gamma}$ change. The spindle speeds $s_1 = 14$ min^{-1} and $s_2 = 110$ min^{-1} are chosen for the experimental measurement. These spindle speeds correspond to the shear rates $\dot{\gamma}_1 = 13.03$ s^{-1} and $\dot{\gamma}_2 = 102.37$ s^{-1}. The Mohr-Westphal balance is used to determine the dependence of the oil density ρ_O on the temperature t_O [3].

2.2 Evaluation of experimental measurement

The experimentally determined dependence of the oil dynamic viscosity η_O on the temperature t_O is shown in Fig. 1. The experimentally determined dependence of the oil density ρ_O on the temperature t_O is shown in Fig 2.

* Corresponding author: tomas.polasek@vsb.cz

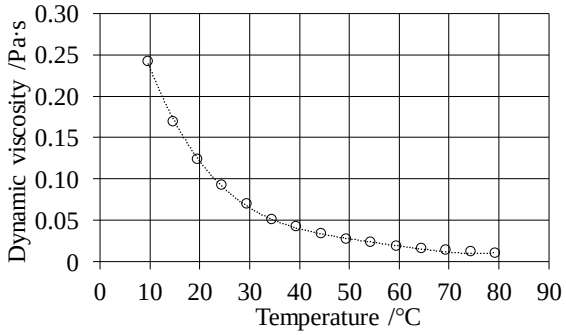

Fig. 1. Dependence of the oil dynamic viscosity η_O on the temperature t_O.

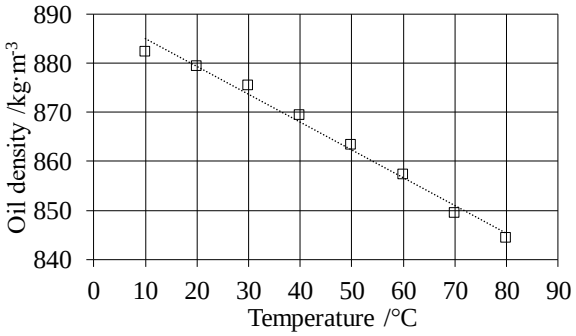

Fig. 2. Dependence of the oil density ρ_O on the temperature t_O.

Both dependencies have the decreasing character when the oil temperature t_O is increased [4]. These obtained oil parameters allow us to define the liquid in the numerical simulation.

The experimentally determined dependence of the shear stress τ_O on the temperature t_O is shown in Fig. 3. In Fig. 4, the experimentally determined dependence of spindle torque T on the oil temperature t_O is shown.

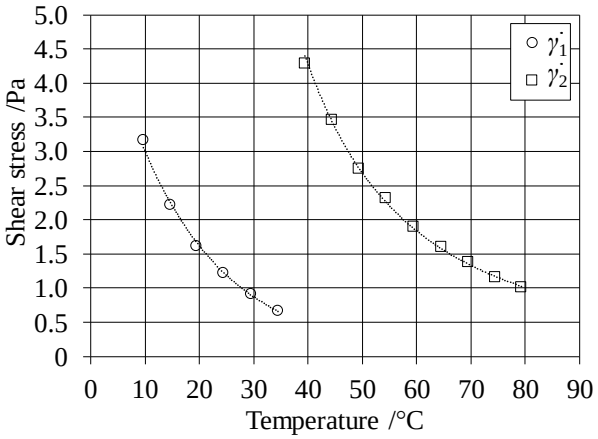

Fig. 3. Dependence of the oil shear stress τ_O on the temperature t_O, the shear rates are $\dot{\gamma}_1 = 13.03\ s^{-1}$ and $\dot{\gamma}_2 = 102.37\ s^{-1}$.

The decreasing dependence of the oil shear stress τ_O and the spindle torque T with the increasing temperature t_O can be observed in Fig. 3 and Fig. 4. The oil dynamic viscosity η_O decreases with the increasing oil temperature t_O. The minimal spindle torque $T_{\%} < 10$ % is reached at the oil temperature $t_O = 40$ °C and the spindle speed $s_1 = 14\ min^{-1}$ ($\dot{\gamma}_1 = 13.03\ s^{-1}$) during the oil dynamic viscosity η_O measurement. For this reason, the spindle speed s is increased to the speed value $s_2 = 110\ min^{-1}$ ($\dot{\gamma}_2 = 102.37\ s^{-1}$).

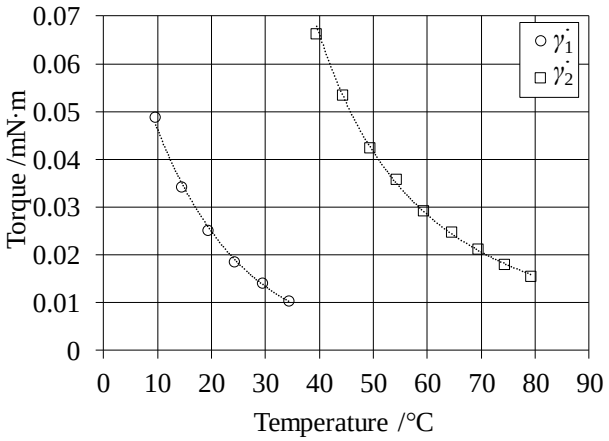

Fig. 4. Dependence of the spindle torque T on the oil temperature t_O, the shear rates are $\dot{\gamma}_1 = 13.03\ s^{-1}$ and $\dot{\gamma}_2 = 102.37\ s^{-1}$.

The dependence of the oil shear stress τ_O and the spindle torque T on the oil temperature t_O is simulated using the numerical simulation.

3 Numerical simulation

3.1 Inverse geometry and computational mesh

The DesignModeler environment is used to modify the inverse geometry. Fig. 5 shows the geometry of the solved region which is formed by the rotating spindle and the container. The structured computational mesh is also shown in Fig. 5. The mesh approximately contains 900 000 elements and it is mainly made up of hexahedron elements. In the region of the largest flow restriction, the computational mesh (dimension $a = 1.14$ mm) is designed to contain 25 elements in the row. The largest refinement of the mesh is created in the gap near the rotating wall.

3.2 Boundary conditions and mathematical model

The boundary condition stationary wall is defined on the inner container wall 1, see Fig. 5.

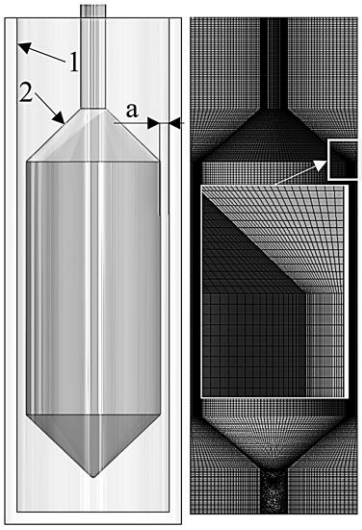

Fig. 5. The solved region and the computational mesh.

On the spindle wall 2, the boundary condition rotating wall is defined. The rotary wall speeds s_1 = 14 min^{-1} and s_2 = 110 min^{-1} are set at this boundary condition. These spindle speeds correspond to the shear rates $\dot{\gamma}_1$ = 13.03 s^{-1} and $\dot{\gamma}_2$ = 102.37 s^{-1}. The axis and the direction of the rotation are also specified.

The density ρ_O and the dynamic viscosity η_O of the flowing liquid are defined for the oil temperature range t_O = (10 ÷ 80) °C. These parameters are determined experimentally, see Chapter 2.2. The mineral oil flows in the gap between the rotating spindle wall and the inner container wall. In this case, the mineral oil flow has the laminar character. The laminar model is used in the numerical simulation.

3.3 Evaluation of numerical simulation

Fig. 6 shows the geometry example of the rotating spindle in the container.

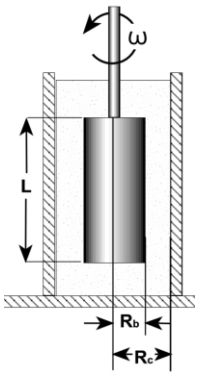

Fig. 6. The spindle and container dimensions [5].

The shear rate $\dot{\gamma}$ is formulated for the cylindrical spindle in the following equation [5]:

$$\dot{\gamma} = \left[\frac{2 \cdot {R_C}^2 \cdot {R_B}^2}{x^2 \cdot \left({R_C}^2 - {R_B}^2\right)} \cdot \frac{2\pi}{60}\right] \cdot s, \qquad (2)$$

where R_C = 9.525 mm is the container radius, R_B = 8.385 mm is the spindle radius, x is the radius at which the shear rate $\dot{\gamma}$ is calculated, s is the spindle speed. The shear rate $\dot{\gamma}$ of the used spindle deals with the equation [2]:

$$\dot{\gamma} = 0.93 \cdot s. \qquad (3)$$

The resulting shear rate $\dot{\gamma}$ and shear stress τ_O are determined for the spindle wall near the gap.

Table 1. The shear rate $\dot{\gamma}$ results according to the equation (3)

	s_1 = 14 min^{-1}	s_2 = 110 min^{-1}
$\dot{\gamma}$ [s^{-1}]	13.03	102.37

The subsequent evaluation of the oil shear stress τ_O is performed for the spindle wall near the gap. The resulting oil shear stresses τ_O for the temperature range t_O = (10 ÷ 80) °C are shown in Fig. 7. The spindle torque T results depending on the oil temperature t_O are shown in Fig. 8. Simultaneously, the simulation results and measurement results are compared in Fig. 7. and Fig 8.

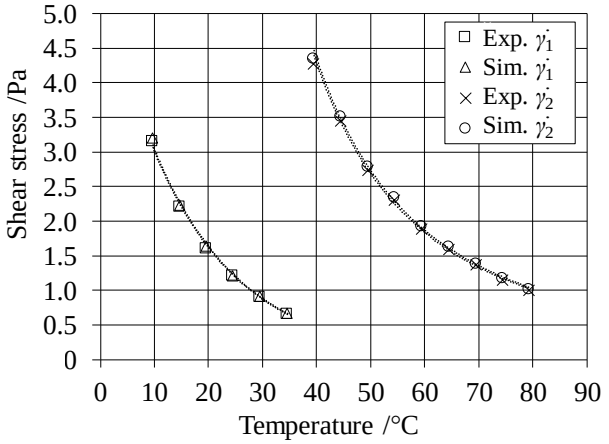

Fig. 7. Comparison of the numerically simulated oil shear stress τ_O depending on the temperature t_O with the experiment.

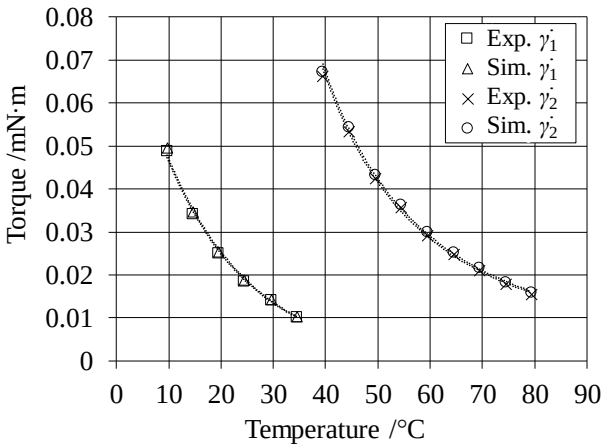

Fig. 8. Comparison of the numerically simulated spindle torque T depending on the temperature t_O with the experiment.

The oil shear stress results τ_O, determined by the numerical simulation, achieve the match with the experimentally determined results. The spindle torque results T, determined by the numerical simulation, also correspond to the experimental measurement.

The numerically simulated contours of oil shear stress τ_O on the spindle wall and the contours of the velocity v in the XY plane are shown in Fig. 9.

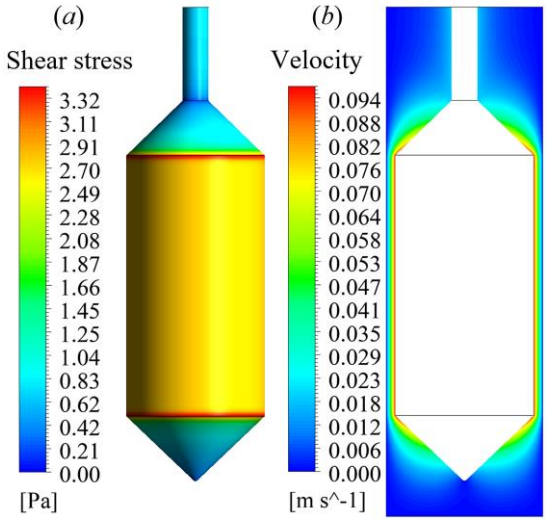

Fig. 9. The oil shear stress τ_O contours on the spindle wall (*a*), the velocity v contours in the XY plane (*b*).

The numerically simulated contours of the shear rate $\dot{\gamma}$ on the spindle wall and in the XY and XZ plane are shown in Fig. 10. The graphical evaluation of the numerical model is done for the oil temperature t_O = 50 °C and the spindle speed s_2 = 110 min^{-1} in Fig. 9 and Fig. 10.

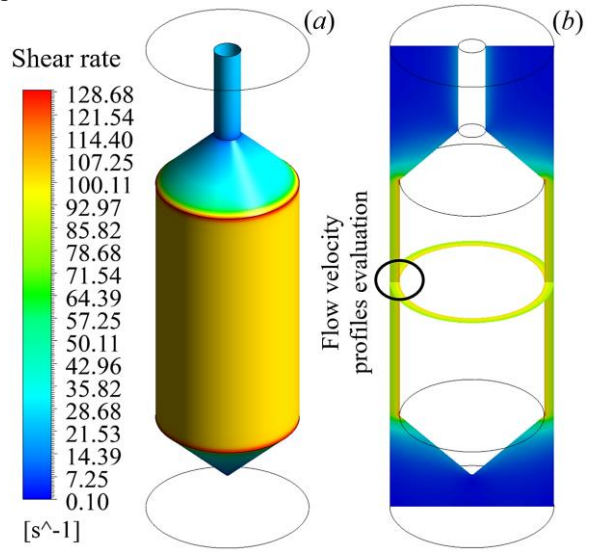

Fig. 10. The shear rate $\dot{\gamma}$ contours on the spindle wall (*a*), in the XY and XZ plane (*b*).

In Fig. 11 and Fig. 12, the numerically simulated flow velocity profiles in the gap are shown. The figures show the influence of the rotating spindle on the oil flow velocity profile.

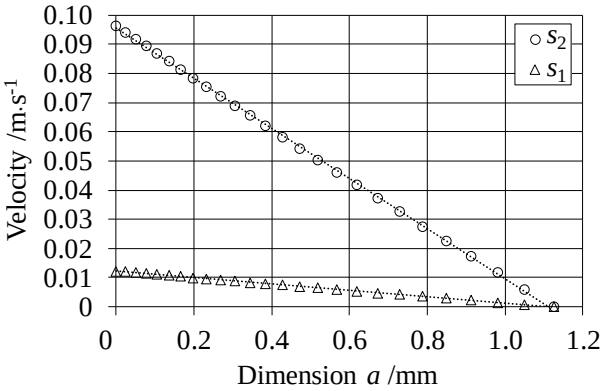

Fig. 11. The oil flow velocity profile in the gap for the spindle speeds s_1 = 14 min^{-1} and s_2 = 110 min^{-1}.

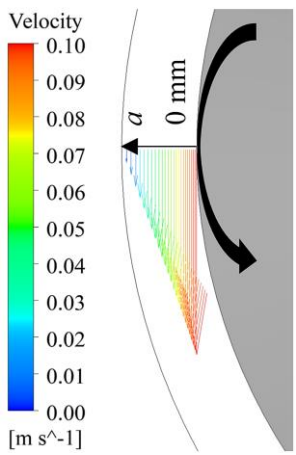

Fig. 12. The oil flow velocity profile in the gap for the spindle speed s_2 = 110 min^{-1}.

Conclusions

The influence of the temperature on the shear stress during mineral oil flow and the rheometer spindle torque during its rotation was numerically simulated in this article. The experimentally determined results of the oil density and the oil dynamic viscosity dependence on the temperature were summarized in the article. The dependence of the oil shear stress and the rheometer spindle torque on the temperature was also measured. Both these quantities decreased with the increasing oil temperature. The mathematical model of the flow was created in the ANSYS Fluent environment. Then the numerical simulation results were compared with the experimentally achieved results. The match of the numerical simulation and the experimental measurement was achieved.

This work was supported by the European Regional Development Fund in the Research Centre of Advanced Mechatronic Systems project, project number CZ.02.1.01/0.0/0.0/16_019/0000867 within the Operational Programme Research, Development and Education.
This work has been supported by The Ministry of Education, Youth and Sports of the Czech Republic from the Specific Research Project SP2019/123 (Numerical Modelling of Dynamic Phenomena in Fluid Mechanics with Support of Experimental Research).

References

1. M. Kozdera, and S. Drábková, Numerical modelling of the flow in the annular multi-recess hydrostatic thrust bearing using CFD methods. *The European Physical Journal*. 2013, Vol. 45. ISSN 2101-6275
2. Brookfield Engineering Laboratories, Inc., Brookfield DV-II+Pro Programmable Viscometer, Operating Instructions
3. T. Polášek, A. Bureček, and L. Hružík, EPJ Web of Conferences, EFM18, *Mathematical simulation of the temperature influence on pressure drop at pump suction line*, **213**, 02069, (2019)
4. D. Knežević, V. Savić, FACTA UNIVERSITATIS, Mechanical Engineering, *Mathematical modeling of changing of dynamic viscosity, as a function of temperature and pressure, of mineral oils for hydraulic systems*, **4** (1), 27-34 p., (2006)
5. Brookfield Engineering Laboratories, Inc., More Solutions to Sticky Problems, A Guide to Getting More from Your Brookfield Viscometer